Acta Materialia 168 (2019) 87–99

Contents lists available at ScienceDirect

Acta Materialia

journal homepage: www.elsevier.com/locate/actamat

Full length article

Comparison between stress-strain plots obtained from indentation plastometry, based on residual indent profiles, and from uniaxial testing

J.E. Campbell, R.P. Thompson, J. Dean, T.W. Clyne*

Department of Materials Science & Metallurgy, Cambridge University, 27 Charles Babbage Road, Cambridge, CB3 0FS, UK

ARTICLE INFO

Article history:
Received 28 November 2018
Received in revised form
5 February 2019
Accepted 6 February 2019
Available online 14 February 2019

Keywords:
Indentation
Inverse FEM
Profilometry
Residual indent profiles

ABSTRACT

This paper is focused on comparisons between stress-strain plots from conventional uniaxial (tensile or compressive) testing and those obtained from indentation experiments, via iterative FEM modeling of the process in which the plasticity is represented using a constitutive law. Both Ludwik-Hollomon and Voce equations are used in the current work. Advantages of a spherical indenter shape, and of using the residual indent profile as the main experimental outcome, are highlighted. It is shown via detailed study of two different materials, with low and high work hardening rates, that the methodology (here termed indentation plastometry) can be used to obtain (nominal) tensile stress-strain curves, which incorporate the onset of necking and the ultimate tensile strength. High levels of fidelity are observed between these and corresponding plots obtained by conventional tensile testing. It is noted that, while there is also excellent consistency with the outcomes of uniaxial compression tests, the latter inevitably involve some experimental complications that are best avoided. It is concluded that indentation plastometry has the potential to become a mainstream testing methodology in the near future.

© 2019 Acta Materialia Inc. Published by Elsevier Ltd. All rights reserved.

1. Introduction

Iterative FEM simulation of the indentation process has enormous potential for extraction of bulk mechanical properties, but there are various unresolved questions relating to optimization of its efficiency and reliability. The methodology, as applied to the extraction of plasticity characteristics, is here termed indentation plastometry. Several recent publications [1–6] highlight issues that need to be taken into account. Software packages are now starting to become available that allow automated extraction of properties from experimental indentation data. In view of the major advantages offered by indentation, compared with conventional testing procedures, these developments are likely to have far-reaching consequences. Of course, clear confirmation of accuracy, reliability and robustness will be essential in order for these to materialize.

Several key points have emerged. For example, the advantages of a spherical indenter shape are compelling [3–5,7,8]. Furthermore, it is now widely understood that, if bulk properties are required, then the deformed region must be large enough for its response to be representative of the bulk. For the majority of polycrystalline (metallic) materials, with grain sizes typically of at least a few tens of microns, this translates into minimum indent depths of this order and minimum indent diameters of hundreds of microns. Moreover, since plasticity characteristics would normally be required that are reliable up to strains of at least, say, 15–20%, the indentation process must generate strains of at least this magnitude, which might typically translate into a depth/indenter radius ratio ("penetration ratio") of a similar order [5], although exact values depend on plasticity characteristics.

The upshot of these requirements is a need for indenters with diameters of the order of 1 mm and for loading systems with capabilities up to the kN range. Most "nanoindentation" systems are thus completely unsuitable. It seems clear that physical set-ups need to be developed that are tailored for this purpose, and that these are likely to be closer in appearance and scale to a conventional hardness testing machine than to a "nano-indenter". Fortunately, this is likely to mean that typical costs are closer to those of the former, rather than those of the latter.

There are, however, a number of slightly more subtle points that need to be addressed if these procedures are to become widely

* Corresponding author.
E-mail address: twc10@cam.ac.uk (T.W. Clyne).

https://doi.org/10.1016/j.actamat.2019.02.006
1359-6454/© 2019 Acta Materialia Inc. Published by Elsevier Ltd. All rights reserved.

utilized. These include the optimum type of indentation data to be employed and the best experimental procedures for obtaining them. Most previous work has been based on load-displacement data, obtained during the indentation test. This brings certain requirements, relating both to the experimental set-up and to the way that the FEM modeling is carried out. Of course, in any event, the resolution of the experimental measurements needs to be relatively high. This is a consequence of a basic feature of iterative convergence on the "optimum" set of plasticity parameters, which is that there is a danger of "compensation" - ie an error in the deduced value of one of the parameters being largely cancelled out by a (compensating) error in another of them, so as to give a similar outcome to the indentation test. This is sometimes expressed as a problem of a potential lack of "uniqueness" for the obtained solution.

There is also the related issue of an algorithm for efficient scanning of parameter space, so as to converge rapidly on the optimum "solution". Several have been proposed [6,9–12], with a variant of the well-known Nelder-Mead algorithm having been shown [5] to be very effective in this context (when combined with a suitable "goodness-of-fit" parameter). This work produced inferred stress-strain curves lying within ±5%, over the complete strain range, of those obtained by uniaxial testing, for all of the (5) materials tested (covering a wide range of plasticity characteristics).

However, even with such an algorithm, if the experimental data are of relatively low accuracy, and/or cover a limited range, then the inferred property parameter values may be unreliable. Testing on a relatively coarse scale does bring important advantages in this respect, since it reduces the requirement in terms of the absolute resolution of the displacement measurements, as well as reducing the errors likely to arise from surface roughness, oxide layers etc. Nevertheless, there is likely to be at least some noise in the displacement data. Moreover, there will often be concerns about the effect of the compliance [13–16] of the loading train: this contribution to the measured displacement must be subtracted, since it cannot be included in universal software for modeling of the indentation process.

While the above issues do not constitute insuperable problems, they do present a challenge in terms of the accuracy of displacement data. In practice, getting these errors significantly below, say, ±1% is difficult. The measurement of load, on the other hand, is simpler, with the accuracy of load cells normally being better than this, and with fewer potential sources of complication. It has been recognized for some time that there is an obvious alternative dataset that can be used, which is the profile of the residual indent. These have been used (in isolation) to infer plasticity parameters [16–18], although this has not been very common so far.

There is a strong incentive to explore this option in more detail, since it offers important advantages. It means that no measurements at all need to be made during the actual test, apart from noting the final value of the load. There need also be no concerns about compliance. These could be critical advantages in some situations, such as for *in situ* field testing of components. It naturally requires a procedure for (accurate and reasonably rapid) profile measurement. However, this also is easier when the scale of the indent is relatively coarse and there are certainly some established (mechanical and optical) profilometry techniques that are likely to give the required resolution and ease of measurement.

Quite separate from these issues relating to indentation plastometry, care must also be taken in interpretation of the outcome of conventional uniaxial testing, both tensile and compressive. In addition to potential difficulties with accurate displacement measurement, and a possible requirement for a compliance correction, it must be recognized that the standard conversion between nominal and true stress-strain relationships is only reliable if the stress and strain fields are uniform (throughout the gauge length). In tension, the onset of necking will invalidate this assumption, so it is important to be able to identify this transition. In some cases, when the initial work hardening rate is relatively low, this may occur at low plastic strains. It is possible to model this using FEM (for any given true stress – true strain relationship). There has been work in this area and it is accepted that predicted outcomes [19–21] should be reliable using the boundary condition of no lateral contraction at the gripped regions.

Similarly, there are complications for compressive testing, mainly related to the effect of interfacial friction. This is commonly neglected, but in practice it is difficult to eliminate it, since the contact pressure is so high. A finite value for the coefficient of friction leads to barreling, which in practice is almost invariably observed on samples that have been subjected to compression testing. In such cases, the assumption of uniform stress and strain fields is again invalid, although it is again possible to take its effect into account via FEM modeling [22–29].

Unlike necking during tensile testing, friction during compression always affects the outcome from the start. On the other hand, its effects may be relatively small, whereas necking always has a strong effect on a plot of nominal stress against nominal strain. Nevertheless, automatic conversion of nominal to true stress-strain relationships is potentially unreliable in both cases. Of course, a finite coefficient of friction value is also likely for indentation [30–32].

It is important to recognize the real objective of this whole area of development, which is primarily to obtain (from indentation testing only) an outcome that corresponds to some "gold standard" of conventional testing. Most practitioners would probably see this as a nominal stress v. nominal strain plot obtained during tensile testing, including the "ultimate tensile strength" (UTS). The latter (ie the peak of such a plot) normally corresponds to the onset of necking - or at least it does for metals exhibiting significant plasticity, which covers virtually all those of wide interest for structural purposes. The prime outcome of indentation plastometry is a set of (best fit) parameter values in a constitutive law describing the true stress – true strain plasticity relationship. However, once this relationship has been established, it is a relatively simple matter to use it in a simulation of a tensile test, and hence to obtain the required plot, including the UTS value (and corresponding plastic strain).

There is every prospect of this becoming a routine and reliable operation. More problematic would be to simulate how neck growth and rupture subsequently occurs, partly because this commonly involves cavitation and would not conform to the same (true) stress-strain relationship as during conventional plastic deformation. Obtaining what is sometimes termed a "ductility" (nominal strain at fracture) is thus not within the anticipated scope of the methodology. It should, however, be noted that a ductility defined in this way is in any event not a very meaningful parameter, strongly influenced as it is by how the neck develops and ruptures. The (nominal) strain at the onset of necking, which is obtainable using the methodology, is arguably a more meaningful measure of "ductility".

Finally, in view of the plethora of recent activities in the area, the contribution being made by this particular paper should perhaps be clarified. A sequence of publications by the current authors has focused successively on the basics [2] of iterative FEM simulation of indentation (using load-displacement data), the effect of residual stresses on the indentation response [33], application of the methodology to coatings [34], the attractions of using spherical indenters [4], a method for obtaining strain rate sensitivity parameters via impact indentation [35], optimization of the

convergence procedure [5] and an example industrial application [16] (sprayed superalloy). The current paper presents two main advances - firstly, a detailed critique of the advantages of using the residual profile, rather than the load-displacement plot, and secondly an explanation of how extracted information can be used to create a uniaxial tensile (nominal) stress-strain plot, and of points to be borne in mind when making a comparison with directly-obtained data of this type.

2. Experimental procedures

2.1. Sample preparation

The work described here was carried out using extruded rods (10 mm diameter) of OFHC copper, obtained from a commercial source. It was used in two conditions - as-received (AR-Cu) and after annealing (in a sealed ampoule) to induce recrystallization (Ann-Cu). It was confirmed that the grain size of the AR-Cu was about 30 μm, while that of the Ann-Cu was about 100 μm. Samples for tensile testing were machined to a Hounsfield shape, with a uniform diameter section of 5 mm diameter and 28 mm length. Samples for compressive testing were cylinders of 10 mm diameter and 10 mm length. Surfaces for indentation were polished to a finish of 1 μm for the AR-Cu, using an automatic system to ensure that the polished face was accurately parallel with the base. For the Ann-Cu, which was very soft, there was a danger of the polishing operation leaving a relatively deep work-hardened layer, so prolonged and careful polishing on a 0.25 μm cloth was employed. All testing was carried out at room temperature (22 °C ±2 °C), using an Instron 3367 screw-driven machine with a 30 kN load cell, under displacement control (at a rate of 10 μm s^{-1}).

As was highlighted in earlier work [5], extruded rods can exhibit significant (plastic) anisotropy, as a result of crystallographic texture. Indentation tests generate highly multi-directional strain fields and stress-strain curves obtained from them will always tend to correspond to some sort of direction-averaged version. For present purposes, this can create a complication that is best avoided, so the two materials in the present study were chosen partly because they exhibit very low levels of anisotropy.

2.2. Tensile and compressive testing

For tensile testing, a clip gauge (Epsilon 3442 extensometer) was used for displacement measurement, so that no compliance correction was needed. The "gauge length" (between clip gauge knife edges) during testing was 10 mm. Compression samples were loaded between rigid (hardened steel) platens, with or without MoS_2 lubricant on both platens. The displacement was measured using an eddy current gauge having a resolution of about ±0.25 μm. It was attached to the upper platen and actuated against the lower one. No attempt was made to apply a compliance calibration, because the results were analysed via FEM simulation of the process, incorporating the effect of the (small) compliance of the platens.

A Taylor Hobson (Talysurf) profilometer (ie a contacting stylus), with a wide-range inductive gauge and 2 μm radius cone recess tip, was used to measure barreling profiles along the length of samples after compression testing. The height resolution of these scans is about 2 μm. Tilt correction functions were applied to the raw data.

2.3. Indentation plastometry

The indentation testing was carried out using the same set-up as for compression testing. A spherical indenter of radius 1 mm was employed, made of a WC-Co cemented carbide (cermet). This sphere was located in a matching recess in a steel housing, where it was secured by brazing. Further details are supplied in a recent paper [5]. It was emphasized there that a careful compliance calibration may be necessary when obtaining accurate load-displacement data for indentation plastometry purposes. However, the present work is focused on use of residual indent profiles, so that no measurements (other than noting the maximum load) need to be carried out during the loading operation.

The profilometer employed for barreling characterization was also used to measure residual indent profiles (assumed to be radially symmetric). Scans were carried out in two perpendicular directions, both through the central axis of the indent. The average profile from the two orthogonal scans was used for comparison with predicted profiles. Tilt correction functions were applied to the raw data, based on the far-field parts of the scan being parallel.

3. FEM model formulation issues

3.1. Constitutive laws

Central to the methodology of indentation plastometry is representation of the true stress – true strain relationship (beyond the yield point) by constitutive laws. Several have been proposed, but the most common are those of Ludwik-Hollomon (L-H)

$$\sigma = \sigma_Y + K\varepsilon_p^n \tag{1}$$

where σ is the deviatoric (von Mises) stress, σ_Ψ is its value at yield, ε_p is the equivalent plastic (von Mises) strain, K is the work hardening coefficient and n is the work hardening exponent, and Voce

$$\sigma = \sigma_s - (\sigma_s - \sigma_Y)\exp\left(\frac{-\varepsilon_p}{\varepsilon_0}\right) \tag{2}$$

where σ_s is a saturation level and ε_0 is a characteristic strain for the exponential approach of the stress towards this level.

3.2. Model meshing and boundary conditions

The current work involves FEM simulation, not only of (spherical) indentation, but also of uniaxial (tensile and compressive) testing. The meshes used in all 3 cases are shown in Fig. 1. All three are radially symmetric. In all cases, there is no dependence of the outcome on absolute scale. However, for indentation, both the radial and axial extent of the domain, relative to the indenter radius, need to be large enough to ensure that they do not affect the outcome. (This also needs to be true for the experimental set-up.) It was confirmed that this was the case for the domain shown. For both tensile and compressive testing, there could in principle be a dependence on the aspect ratio, L/r, of the domain. Values of 8 and 4 were used for the tensile testing, while it was fixed at 1 for compressive testing. (The values in the experiments were respectively 6 and 1.) In view of findings from previous work [19–21], a boundary condition of no lateral contraction at the ends of the gauge length was employed for the tensile testing. This affects the onset of necking (the development of non-uniform stress and strain fields). For compressive testing, interfacial sliding between platen and sample was controlled by the value of a coefficient of friction. A non-zero value (ie at least some inhibition of sliding) also tends to create inhomogeneous stress and strain fields. Details about how friction is handled in the model are provided in a previous publication [5].

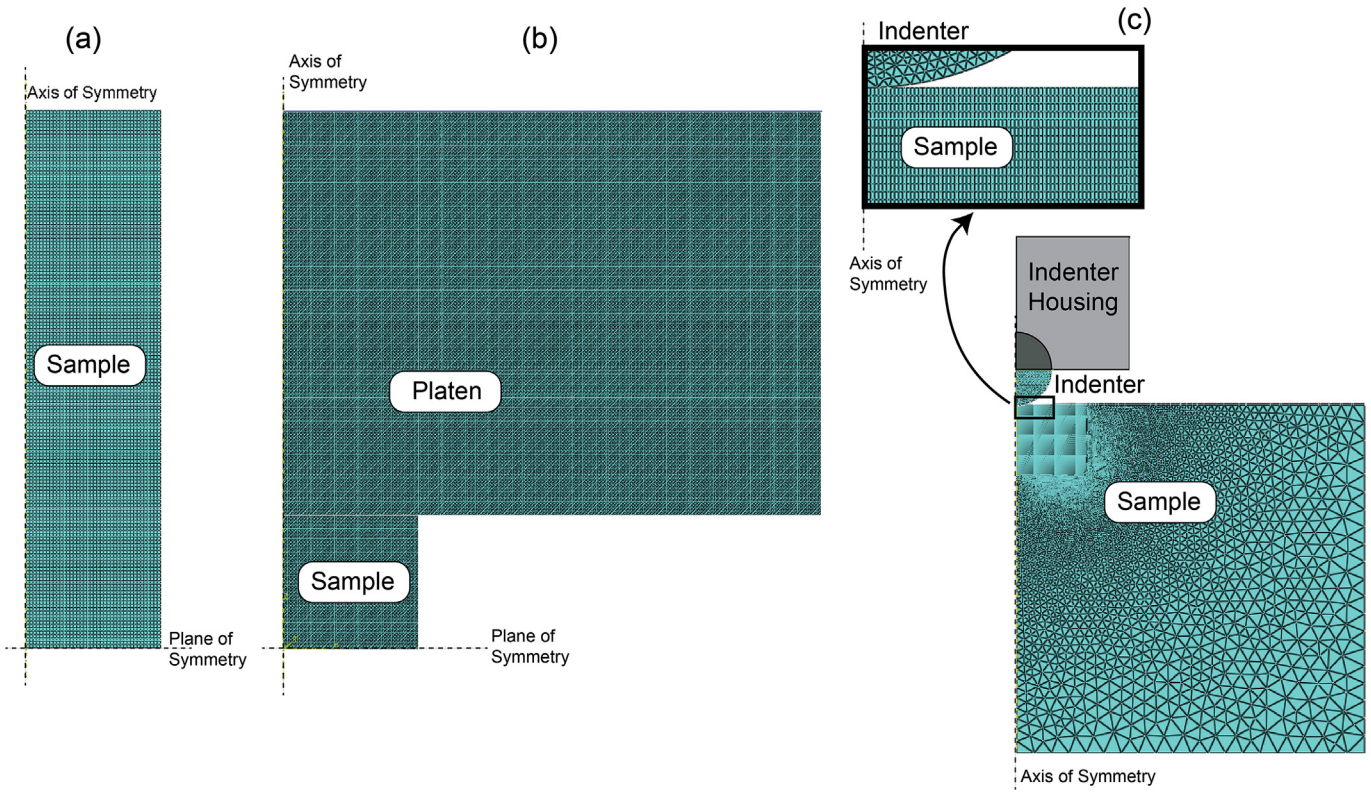

Fig. 1. FEM Meshes for simulation of (a) tension, (b) compression and (c) indentation.

3.3. Convergence algorithm

The algorithm used to converge in parameter space on the best fit combination of (Ludwik-Hollomon or Voce) parameter values is the Nelder-Mead simplex search [36]. This was chosen in view of its robustness and adaptability, particularly with respect to noise. The procedure used is based on that of Gao and Han [37], and was built using the Scientific Python and Numeric Python packages [38,39]. Full details are available elsewhere [5].

The goodness-of-fit between target and modeled data (primarily residual indent profile) is characterized here via a dimensionless parameter S_{red}, a "reduced sum of squares of the residuals". The sum of the squares of the residuals, S, can be expressed in the present case as

$$S = \sum_{i=1}^{N} \left(\delta_{i,\text{M}} - \delta_{i,\text{E}}\right)^2 \tag{3}$$

where $\delta_{i,\text{M}}$ is the ith value of the modeled height difference (predicted by FEM) and $\delta_{i,\text{E}}$ is the corresponding experimental (target) value, while N is the total number of radial locations being considered. Perfect fit will lead to a value of zero for S. Since S is dimensional, it has units and its magnitude cannot be used to give a universal indication of the quality of the fit. For this purpose, the dimensionless quantity S_{red}, a "reduced sum of squares" is used, defined by

$$S_{\text{red}} = \frac{\sum_{i=1}^{N} \left(\delta_{i,\text{M}} - \delta_{i,\text{E}}\right)^2}{N\,\delta_{\text{av,E}}^2} \tag{4}$$

where $\delta_{\text{av,E}}$ is the numerical average of the highest and lowest of the experimentally-measured heights. The value of N was not predetermined, but was dependent on the radial range, which extended to a position such that the height had returned to within 5 μm of the far field level (ie the level of the original flat surface). The interval between radial locations was 10 μm, so that, if the height reached a level within 5 μm of the original surface at a radial distance of, say, 1.6 mm, then the value of N would be 160.

The parameter S_{red} is thus a positive dimensionless number, with a value that ranges upwards from 0 (corresponding to perfect fit). As a generalization, modeling that captures the material plasticity response reasonably well should lead to a solution (set of parameter values) for which S_{red} is less than, say, 10^{-3}. This effectively constitutes a health check on the solution - if, for example, no solution can be found giving a value smaller than, say, 1%, then this suggests that there can only be limited confidence in the inferred set of values. This could be due to experimental deficiencies and/or an inability to capture the behaviour well with the constitutive law being used. In fact, during the work described here, solutions with S_{red} values around 10^{-4} or below were found in all cases. This represents excellent agreement.

4. Uniaxial testing outcomes

4.1. Experimental test results

Tensile stress-strain curves for the two materials are shown in Fig. 2(a), with both nominal and true values plotted, while corresponding compressive curves (with and without lubrication) are plotted in Fig. 2(b). These two materials clearly exhibit very different plasticity characteristics, with the as-received material (AR-Cu) having a relatively high yield stress, but then exhibiting limited work hardening, while the annealed material (Ann-Cu) has a low yield stress, followed by a high rate of work hardening (and

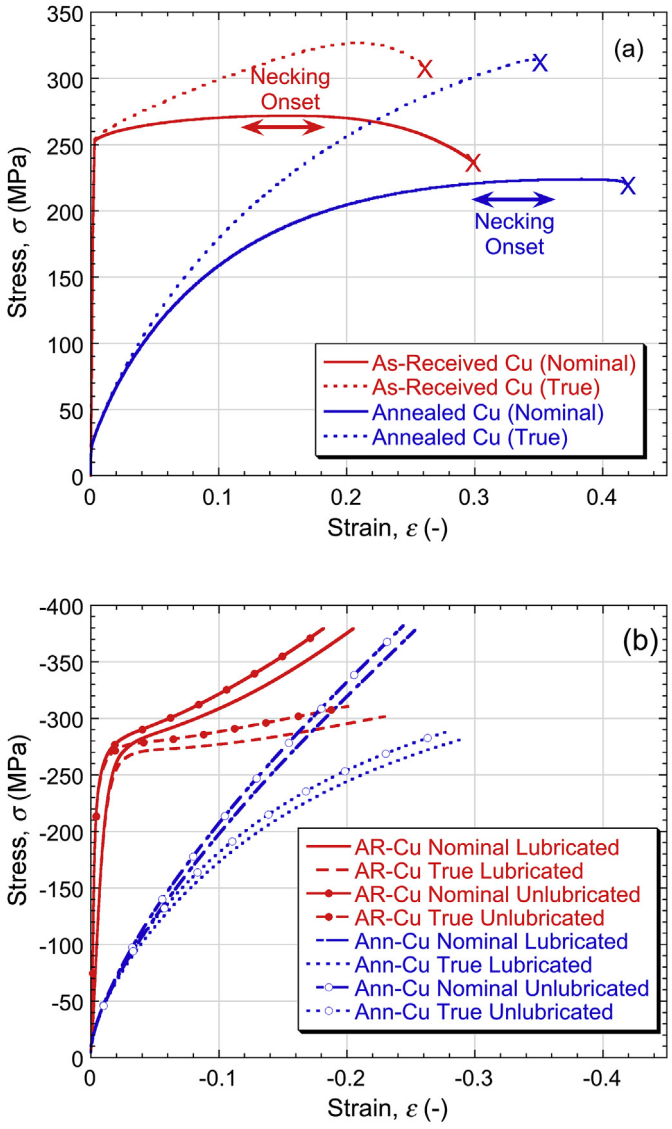

Fig. 2. Experimental uniaxial data (plotted as nominal stress v. nominal strain and true stress v. true strain), for both materials, (a) in tension and (b) in compression (with and without lubrication).

greater ductility in tension).

In tension, necking is expected to start where the nominal plot reaches a peak, or plateau. It can be seen that this occurred at around 13–17% strain for the AR-Cu, giving a UTS of about 270 MPa, while for the Ann-Cu it was at about 30–35% strain (UTS ~230 MPa). Of course, necking tends to start at higher strains for materials with greater work hardening rates. The standard conversion of nominal to true stresses and strains is only reliable up to the onset of necking.

There are also some points to note about the compression results. For example, lubrication clearly does have an effect. In fact, two effects are noticeable. Firstly, the initial ("elastic") slope is lower when lubricant is present, although this is only noticeable for the AR-Cu (with the relatively high yield stress). This is presumably due to a "bedding down" effect, which is more pronounced in the presence of lubricant - probably as a result of it being progressively squeezed out of the interface during the early part of the test. However, even the unlubricated case does show some evidence of such an effect, which can arise if the surfaces coming into contact are not perfectly flat and parallel. Bedding down effects could be avoided by using a clip gauge, but that is difficult for compression testing. Secondly, the absence of lubricant does lead to a (small, but noticeable) progressive increase in the stress needed to continue straining, compared with the lubricated case. This is more noticeable for the Ann-Cu. It is presumably a consequence of the coefficient of friction being higher when there is no lubricant.

Of course, the true stress – true strain curve for any given material should be the same in tension and compression. This is approximately observed here for both materials, but there are a couple of caveats. Firstly, the comparison can only be made up to the point where necking starts in tension, which is at a fairly low strain (~13%) for the AR-Cu. Secondly, in compression there are two complications, one being the "bedding down" effect, which makes accurate identification of the yield stress rather difficult, and the other being that interfacial friction does influence the obtained curve (and is unlikely to be entirely eliminated even with lubrication - see below).

4.2. Modeling of tensile testing

For tensile testing, sets of best fit L-H and Voce parameters were obtained for each material, using Nelder-Mead convergence (on the nominal stress v. nominal strain plot, up to a strain just beyond the onset of necking - ie ~20% for AR-Cu and ~40% for Ann-Cu). The modeled curves are for a sample (uniform diameter section) aspect ratio of 4, although it was confirmed that using a value of 8 gave very similar results. The comparison in Fig. 3(a), between experimental and modeled plots, which was obtained using the (best fit) L-H and Voce parameter values in Table 1, demonstrates that excellent agreement can be obtained (ie that the true stress v. true strain characteristics exhibited by these materials can be well-captured using at least one of these constitutive laws). This is clear from the plots and is confirmed by the values of S_{red} shown in Table 1 - a value below 10^{-3} is regarded as representing good fit and below 10^{-4} is excellent. It can, however, be seen that there are (small) differences between the outcomes with the two types of constitutive law. For the AR-Cu, the L-H law allows slightly better conformity to the experimental outcome (S_{red} value of $10^{-3.97}$, compared with $10^{-3.77}$ for Voce). On the other hand, the behaviour of the Ann-Cu can be captured more faithfully using Voce (S_{red} value of $10^{-3.60}$, compared with $10^{-3.19}$ for L-H). Trying at least these two constitutive laws certainly appears likely to be worthwhile.

These L-H or Voce parameter sets clearly lead to tensile nominal stress – nominal strain curves that are accurate. Not only are the yielding and work hardening well captured, but also the UTS, and the corresponding plastic strain ("ductility"), are reliable. It may be noted, however, that, depending on exactly how the UTS is defined, the best fit L-H set for the Ann-Cu could lead to a noticeable error for this ductility, although the UTS (and the preceding part of the curve) would be accurate.

A further point worthy of note here is the difference, for a given L-H or Voce parameter set (ie a given true stress – true strain curve), between the nominal stress-strain plot obtained by FEM modeling and that resulting from simple use of the analytical relationship between them (which will concern only plastic straining). Such a comparison is shown in Fig. 3(b), for the best fit parameter set in each case. It can be seen that, up to the onset of necking (ie the peak in the plot), the differences are minor, reflecting the uniformity of the strain field up to that point - see §4.4 below. Nevertheless, it is worthwhile to use the FEM tensile model, particularly if there is any interest in the early development of necks.

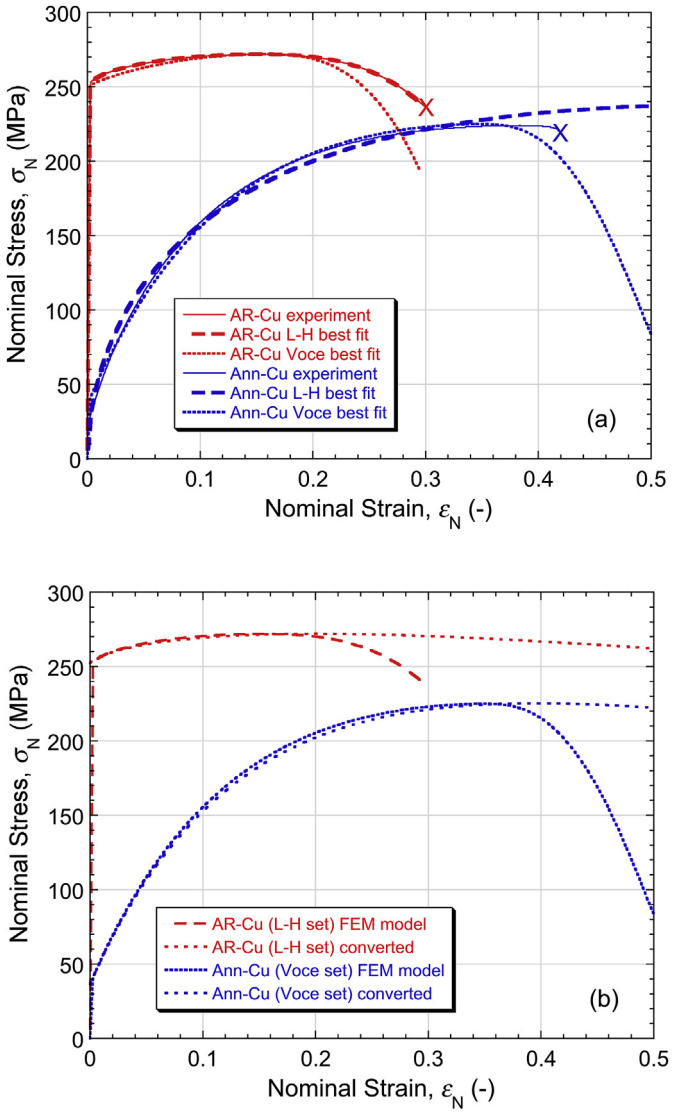

Fig. 3. Nominal tensile stress-strain curves for both materials, showing (a) experimental and FEM modeled plots (obtained using the (best fit) L-H and Voce parameter sets in Table 1) and (b) comparison, based on L-H (AR-Cu) and Voce (Ann-Cu) sets, between the FEM plots and those obtained by direct conversion (using the analytical equations).

Table 1
Best fit (Ludwik-Hollomon and Voce) plasticity parameter values for the two materials, obtained from tensile nominal stress v. nominal strain curves.

Parameter	AR-Cu		Ann-Cu	
	L-H	Voce	L-H	Voce
Yield stress, σ_Y (MPa)	252.5	251.3	0.5	36.9
L-H WH coefficient, K (MPa)	291.1	–	557.5	–
L-H WH exponent, n (–)	0.805	–	0.506	–
Voce saturation stress, σ_s (MPa)	–	461.4	–	375.8
Voce characteristic strain, ε_0 (%)	–	41.1	–	19.5
Misfit parameter, S_{red} (–)	$10^{-3.97}$	$10^{-3.77}$	$10^{-3.19}$	$10^{-3.60}$

4.3. Modeling of compressive testing

For compressive testing, it's clear that friction is relevant, and also that the initial "bedding down" effect presents a complication in terms of comparing model predictions with experiment. There is no real prospect of incorporating the latter into a model, although this can be done for the former (via a coefficient of friction, μ). What has been done here is to use the two best fit sets of parameter values from the tensile comparisons - ie the L-H set for the AR-Cu and the Voce set for the Ann-Cu. There is already at least some information available in the literature about likely values of μ under different conditions, both for (unlubricated) indentation [5,30–32] and for conventional compression [25–29] testing. A value in the approximate range 0.2–0.3 has often been found appropriate for indentation and for unlubricated compression, although clearly there may be a dependence on surface finish, materials etc. During lubricated compression testing, there tends to be more variation, but a value of the order of 0.1 might be considered typical with good lubrication. Accepting that accurate estimation of μ is difficult, and also that it may change during the process, values of 0.1 and 0.3 have been used here, designed to correspond to the lubricated and unlubricated cases. The outcome is shown in Fig. 4. It can be seen that, for both materials, there is at least a measure of agreement between experiment and prediction. The differences between the high and low μ predictions are certainly similar to those of the two experimental conditions. There is clearly an error associated with the "bedding down" process, leading to larger strains over the complete range for the experimental plots. Accepting this, however, and recognizing that, for the most accurate comparisons, it is probably best not to use compressive uniaxial data, the level of consistency is reasonably good (confirming that the plasticity characteristics are being well-captured by these two parameter sets for these two materials).

4.4. Strain fields during uniaxial loading

Confirmation of the dangers of manipulating compressive test data in a simplistic way (converting nominal test data to true stress-strain curves using the analytical equations) is provided by Fig. 5, which shows the plastic (von Mises) strain fields for the 4 cases (two materials, each with the two μ values). Only if these are homogeneous is it safe to carry out such a conversion. It can be seen that this is often not the case, particularly with a high μ value and/or a low work hardening rate (AR-Cu). It is also noteworthy that all

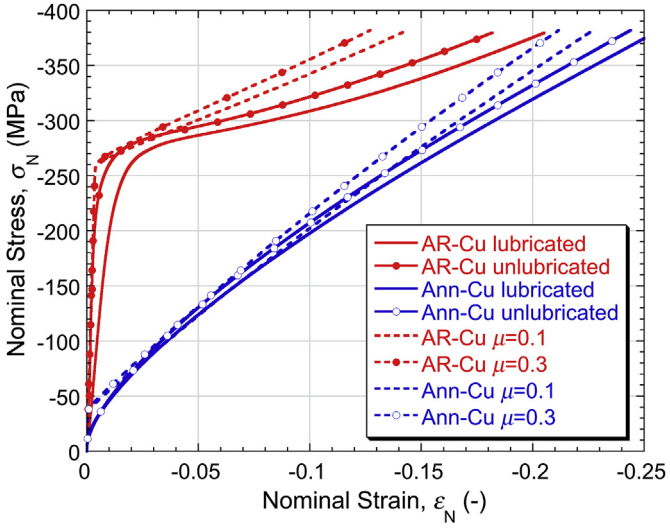

Fig. 4. Comparison between experimental compressive (nominal) stress-strain curves for both materials and corresponding modeled plots, obtained using the L-H parameter values shown in Table 1 for the AR-Cu and the corresponding Voce values for the Ann-Cu.

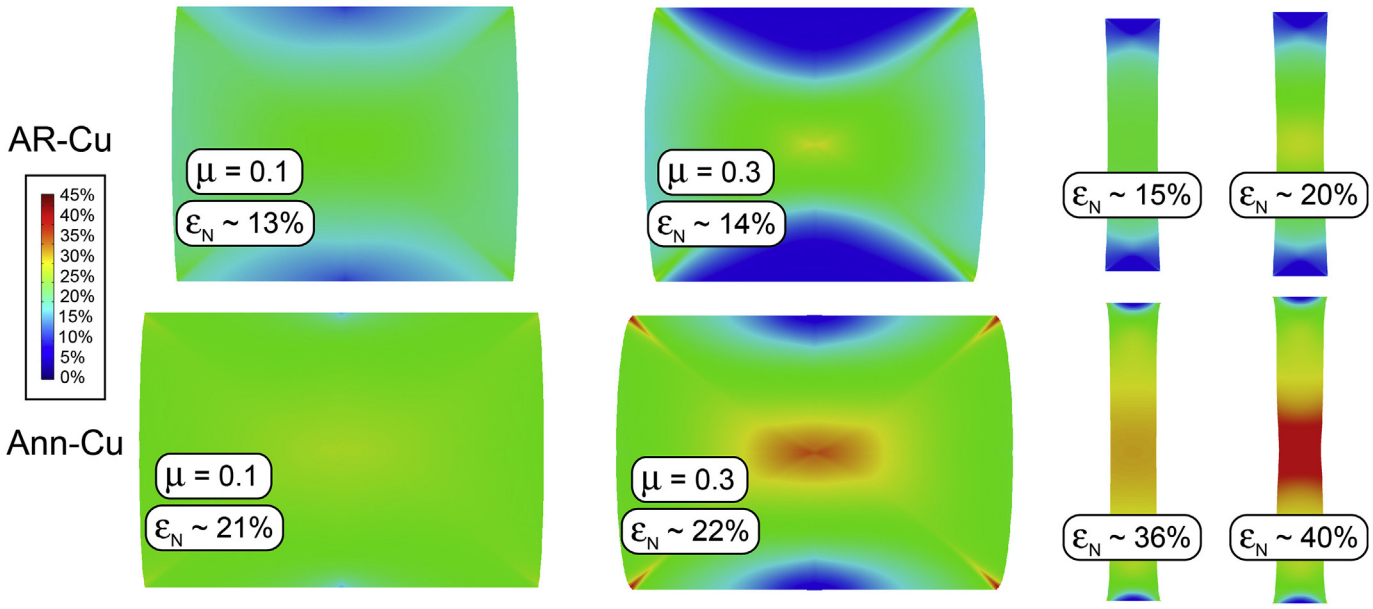

Fig. 5. Predicted (von Mises) plastic strain fields during compressive (left) and tensile (right) loading of the two materials, obtained using the L-H set of plasticity parameters in Table 1 for the AR-Cu and the Voce set in Table 1 for the Ann-Cu.

of these samples are predicted to show significant barreling at the end of the test, particularly with the higher μ value - see §4.5 below.

Also shown in Fig. 5 are the strain fields for tensile testing of these two materials (with an aspect ratio of 4). These are for nominal strains that are around, and also slightly beyond, the onset of necking for the material concerned. These also show some inhomogeneity, although it should be noted that, at the onset of necking, the strain field is quite homogeneous within the gauge length (between the clip gauge knife edges) - at least for the tests carried out here. Of course, as the necks start to develop, these strain fields will become highly inhomogeneous, but modeling of that regime is in any event unlikely to be very reliable (due to the very high strains, and probably cavitation, within the neck). These strain fields do confirm that, up to the onset of necking, conversion between nominal and true stress-strain relationships via the analytical equations should be quite reliable - see Fig. 3(b). Nevertheless, FEM modeling of the tensile test (using indentation-derived sets of plasticity law parameters) is recommended, particularly if at least some indication is required of the behaviour after the onset of necking.

4.5. Barreling profiles after compression testing

Measured barreling profiles are shown in Fig. 6, for both materials, with and without lubrication. Also shown in this figure are corresponding predictions (using the best fit L-H and Voce parameter values) for three values of μ. It can be seen that these data are broadly consistent with μ being about 0.1 for the lubricated case. For the unlubricated case, a value of the order of 0.2 appears broadly appropriate. However, this cannot be regarded as a very accurate way to estimate μ, which in any event is likely to vary from case to case, and perhaps also to change during the process. In particular, these profiles are difficult to capture reliably near the ends of the sample, where the width is changing rapidly. The approach nevertheless gives a broad pointer towards the correct ranges. It may be noted that these effects of friction are separate from those associated with (experimental) "bedding down" effects, which will affect measured stress-strain plots, but not the barreling profiles.

5. Indentation plastometry outcomes

5.1. Microstructural observations

As expected, plastically deformed regions (during indentation) extended over many grains. This is confirmed by Fig. 7, which shows the free surface adjacent to an indent in the as-received material (AR-Cu), for a penetration ratio, δ/R, of 40%. Among the points worthy of note here is the observation of sets of parallel persistent slip bands in each grain, which are physical steps on the surface. It can be seen that, in the majority of grains, at least two slip systems are operative. There are some in which only one set of bands is visible, but of course a slip system in which the slip plane is inclined at a small angle to the free surface would not produce noticeable steps. Since most of the material visible here has undergone relatively low levels of strain (<~few %) - see, for example, Fig. 6 in the previous paper [5] - it is likely that multiple system slip operated virtually from the start in all grains, which is in general expected. Careful inspection of various regions also reveals that some grains have rotated significantly with respect to their neighbours, creating relatively large steps at some grain boundaries. The resistance to this sliding offered by grain boundaries is part of the set of characteristics that dictates the plasticity of the material.

5.2. Sensitivities to profilometry and displacement data

An important objective for indentation plastometry is that of optimizing both the efficiency of convergence on best-fit parameter sets and their reliability in terms of capturing the material response. This will depend to some extent on the constitutive law used, and the convergence algorithm employed, but there is also the issue, for any given outcome (eg a load-displacement plot up to a certain penetration ratio), of how the "goodness-of-fit" varies in parameter space. A sharp peak (at the best-fit "solution", with excellent agreement) will assist rapid and effective convergence,

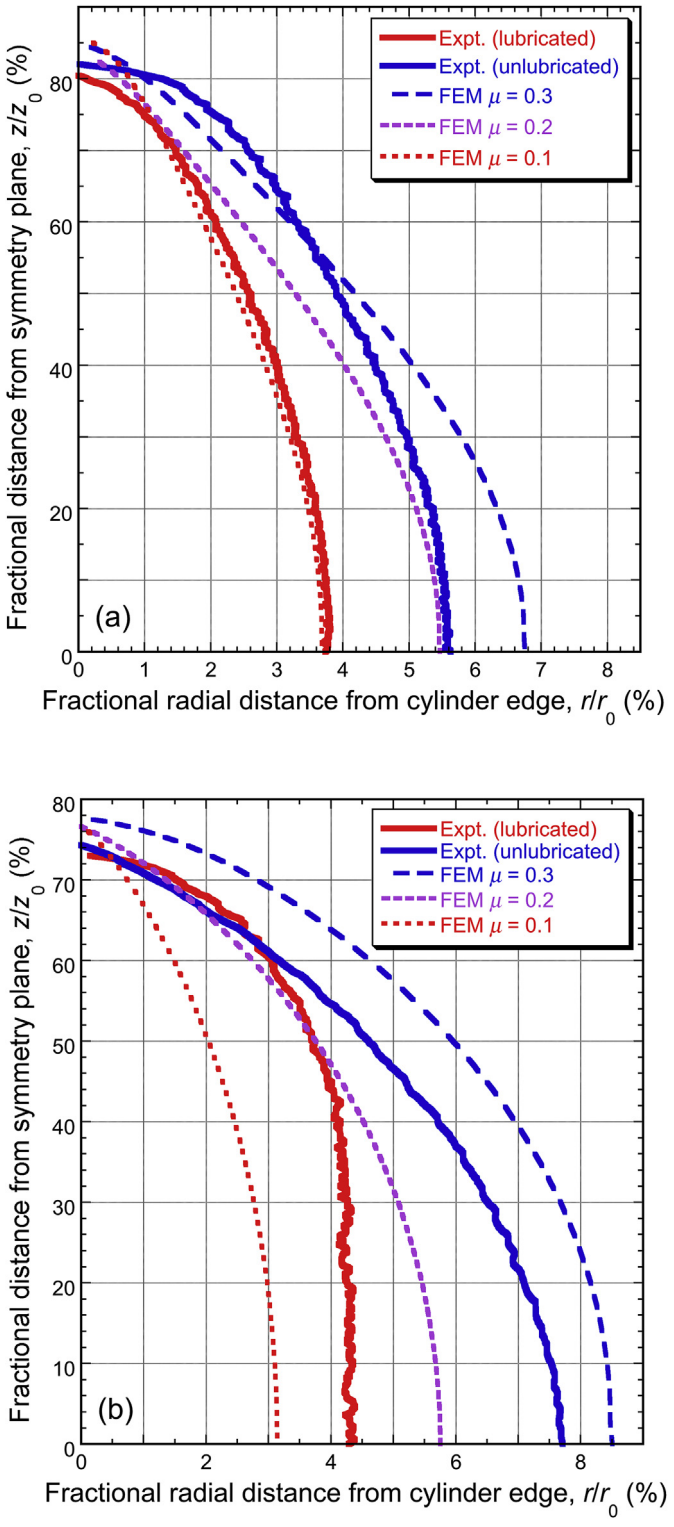

Fig. 6. Comparison between experimental barreling profiles and those obtained via FEM, (a) for AR-Cu (using the L-H set of parameters in Table 1) and (b) for Ann-Cu (using the Voce set in Table 1).

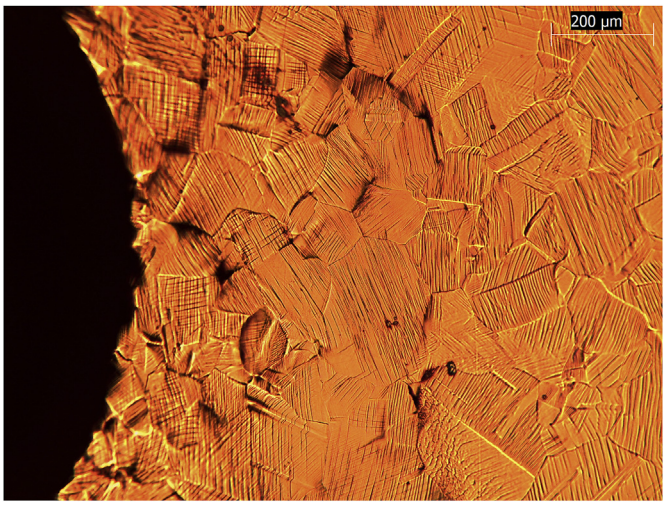

Fig. 7. Optical micrograph of the free surface of an AR-Cu sample, adjacent to an indent of depth about 400 μm.

while a flattish peak, perhaps with extended ridges or undulations, will make it difficult and unreliable.

For purposes of exploring the effect on this sensitivity of selecting different options, such as the choice between using load-displacement data or residual indent profiles, and the effect of having deeper or more shallow penetration, it is preferable to avoid using real experimental data and focus on theoretical outcomes. Extensive investigations of this issue have been carried out, from which a small selection of outcomes is presented here, to illustrate the main conclusions. These relate only to the L-H law, with a fixed value of the work hardening exponent, n. This allows 2-D maps to be created of the value of the misfit parameter, S_{red}, for given combinations of yield stress, σ_Y, and work hardening coefficient, K. This has been done for two "correct" sets of values (representing cases with low and high work hardening rates), which are specified in the figure captions.

Fig. 8 shows the outcome of such an investigation for a low work hardening material (such as AR-Cu). In all cases, there are "ridges" in this parameter space, representing a "compensation" effect - ie if σ_Y is lower than the "correct value (245.6 MPa here), then fairly good agreement can still be obtained via a compensatory increase in K (and vice versa). However, it can be seen that the length (and the "gradients") of these ridges vary between these 4 cases. It is clear that it is preferable to use profilometry data, since the ridges are then much less extensive (ie the sensitivity of the outcome to the stress-strain relationship being represented is stronger). Unsurprisingly, it is also preferable to penetrate more deeply, although it should be borne in mind that outcomes then tend to become more sensitive to the response of the material at very high strains, which may in practice be of limited relevance to the behaviour being characterized. Furthermore, the influence of the friction coefficient tends to be greater for deeper penetration.

Corresponding plots for a higher work hardening material (such as Ann-Cu) are shown in Fig. 9. The higher work hardening rate gives greater scope for compensation effects, and hence the ridges are longer, but in general the same trends are apparent. The profilometry is again more sensitive, with deeper penetration having a slightly greater effect on it than for the AR-Cu. A clear outcome of these studies is that it is preferable to use profilometry data, particularly since it also has the advantage that no measurements of any type are necessary during the test, and there is no need to make any compliance corrections. The optimum penetration ratio will clearly be some sort of compromise value, but greater depths do bring advantages in terms of sensitivity and a value of at least about 20% is likely to be recommended. If load-displacement data are being used, then a significantly larger value than this is likely to be required.

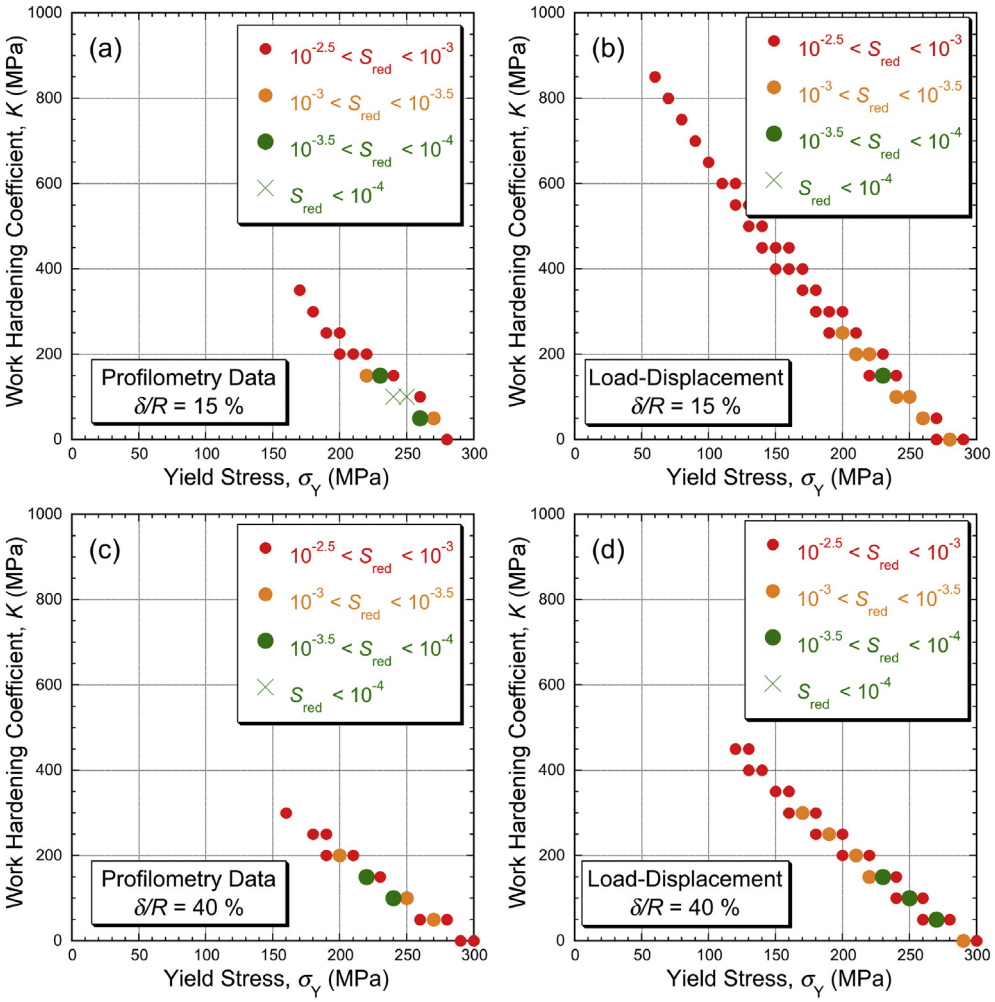

Fig. 8. Goodness-of-fit maps for a low work hardening material (such as AR-Cu), showing S_{red} for various σ_Y and K combinations, when outcomes are compared with those for a "correct" pair of 245.6 and 102.9 MPa respectively, with n fixed at 0.4 (and μ fixed at 0.2). The maps are for (a) δ(r) data, at 15% penetration, (b) P(δ) data, at 15% penetration, (c) δ(r) data, at 40% penetration and (d) P(δ) data, at 40% penetration.

5.3. Stress-strain curves inferred from indentation data

In view of the observations reported in §5.2, attention has been focused on use of profilometry data to infer sets of plasticity parameter values. The best fit sets are shown in Table 2, together with corresponding goodness-of-fit values. These are all sufficiently low for justify confidence in the fidelity with which the plasticity characteristics are being captured. An idea of how these values relate to actual indent profiles can be obtained from Fig. 10, which relates to both materials and to two different penetration ratios. The tendency for more pronounced pile-ups (with high local plastic strains) to be created when the material exhibits little work hardening is clearly apparent. This region is particularly important in terms of a requirement for the profile to be measured with high accuracy.

Once the best fit set of plasticity parameter values has been identified in this way, it can be used in simulation of a tensile test and the outcome compared with the plot obtained in such a test. Such a comparison is shown in Fig. 11, for both materials. Several points should be noted about this comparison. Firstly, the level of agreement is very good regarding the yield stress, the work hardening behaviour and the peak stress (UTS). These are the key mechanical characteristics. What appears to be just slightly less reliably obtained via indentation, particularly for the AR-Cu (low work hardening), is the strain at which the peak stress is created (onset of necking) and the strain at which final fracture occurs.

It should, however, be recognized that both of these, particularly the latter, are of little real significance. The (apparent) strain at fracture is strongly influenced by how the neck develops and ruptures. This is virtually impossible to model reliably and will tend to vary from test to test. It is not a "genuine" strain of any significance. Even the strain at which necking starts is difficult to identify accurately, although it is captured well (at about 30–35%) for the Ann-Cu. For the AR-Cu, there appears to be a slight discrepancy, since the value during the tensile test is around 15%, whereas the indentation-inferred value is about 10%. However, this type of uncertainty will always tend to arise with a material exhibiting a relatively low rate of work hardening (such as this AR-Cu). Such materials are prone to early necking, with the (nominal) fracture stress sometimes being quite close to the yield stress and the exact strain at which necking and fracture occurs tending to be quite variable from test to test. Nevertheless, the indentation-derived plot does reliably capture all of the features that are genuinely important - ie the yield stress, the (low) work hardening rate and the UTS. Incidentally, these FEM outcomes regarding the onset of necking agree well with the Considère construction, which predicts necking when the true stress reaches the gradient of the true stress – true strain curve or, equivalently, at the peak of the nominal

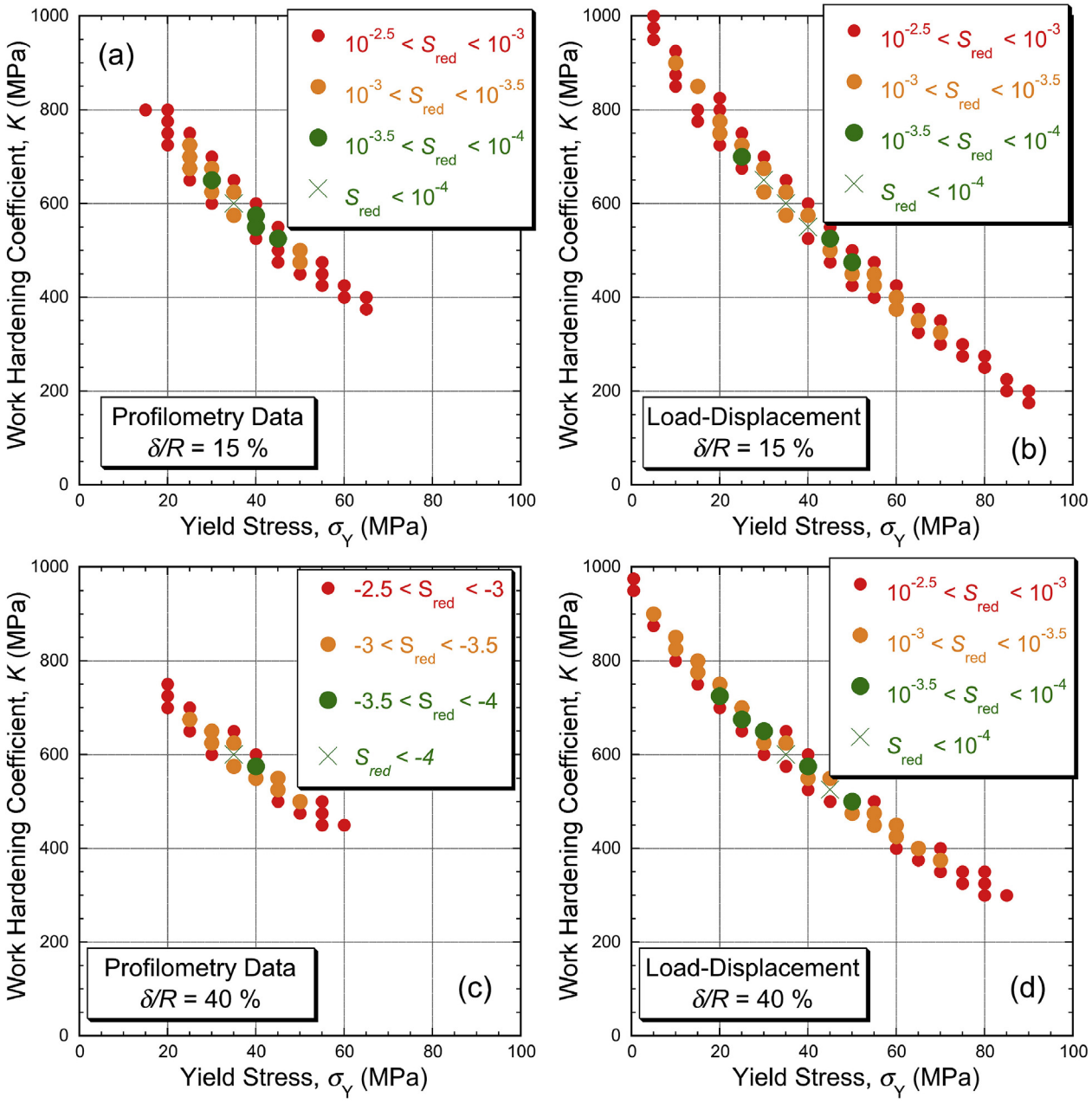

Fig. 9. Goodness-of-fit maps for a high work hardening material (such as Ann-Cu), showing S_{red} for various σ_Y and K combinations, when outcomes are compared with those for a "correct" pair of 36.6 and 593.4 MPa respectively, with n fixed at 0.63 (and μ fixed at 0.2). The maps are for (a) δ(r) data, at 15% penetration, (b) P(δ) data, at 15% penetration, (c) δ(r) data, at 40% penetration and (d) P(δ) data, at 40% penetration.

Table 2
Best fit (Ludwik-Hollomon and Voce) plasticity parameter values for the two materials, for shallow and deep penetration, obtained from indentation profiles.

Parameter	AR-Cu		Ann-Cu	
	δ/R ~20%	δ/R ~40%	δ/R ~20%	δ/R ~40%
L-H Yield stress, σ_Y (MPa)	258.1	237.7	43.5	41.7
L-H WH coefficient, K (MPa)	200.6	221.2	569.9	543.6
L-H WH exponent, n (–)	0.674	0.536	0.635	0.633
L-H Misfit parameter, S_{red} (–)	$10^{-4.16}$	$10^{-4.56}$	$10^{-4.05}$	$10^{-4.80}$
Voce Yield stress, σ_Y (MPa)	266.8	249.7	48.9	46.2
Voce saturation stress, σ_s (MPa)	421.4	468.0	354.9	358.7
Voce characteristic strain, ε_0 (%)	53.2	41.1	16.6	16.5
Voce Misfit parameter, S_{red} (–)	$10^{-4.17}$	$10^{-4.52}$	$10^{-4.31}$	$10^{-4.69}$

stress – nominal strain curve. It should be recognized, however, that, particularly for a material with a low work hardening rate, this peak is often very flat, rendering identification of the strain at the onset of necking rather inaccurate. A comparison of FEM necking outcomes with the Considère criterion is available in an educational software package (https://www.doitpoms.ac.uk/tlplib/mechanical_testing_metals/necking.php).

It may also be noted in Fig. 11 that, as would be hoped, the indentation plastometry outcome is not very sensitive to the penetration depth (between about 15% and 40%). Two caveats should, however, be appended to this observation. One is that very shallow penetration (δ/R <~10%) may result in reduced accuracy for the outcome, particularly if there is interest in the behaviour at high strains. The other is that very deep penetration (δ/R >~40%), while it

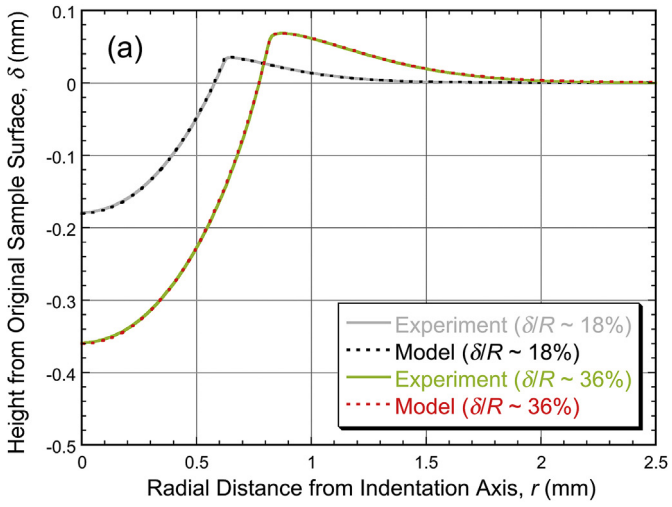

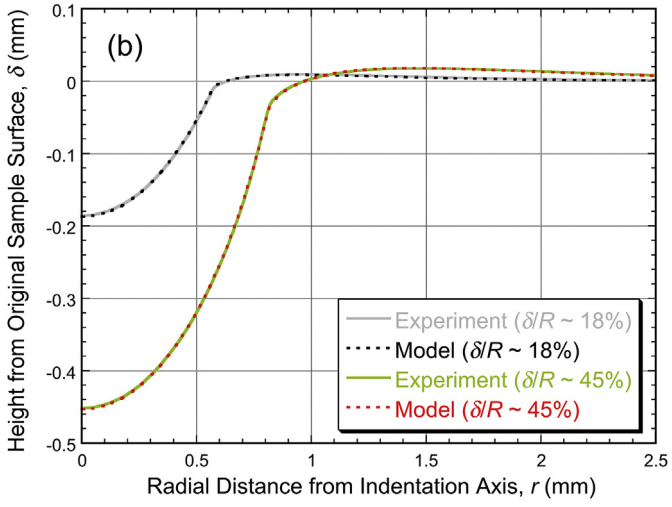

Fig. 10. Measured and (best-fit) modeled residual indent profiles, with shallow and deep penetration, and the value of μ fixed at 0.2, for (a) AR-Cu and (b) Ann-Cu.

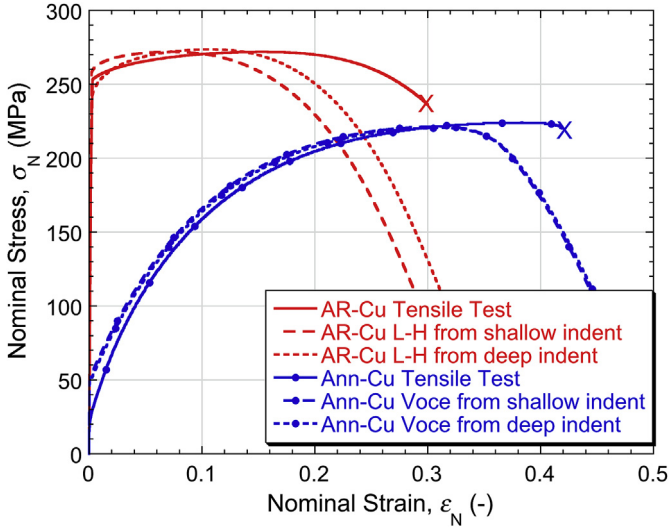

Fig. 11. Comparisons, for both materials, between tensile nominal stress v. nominal strain plots obtained by direct measurement and via iterative FEM targeted on measured residual indent profiles, with inferred best fit plasticity parameter sets (Table 2) being used in FEM simulation of the tensile test.

might assist in rapid convergence, could lead to plasticity parameter sets that are strongly influenced by the behaviour at large strains, which may be of little significance if fracture during tensile testing takes place at substantially lower strains. Of course, it must always be recognized that no material is likely to conform very accurately to any constitutive law over a wide range of strain.

An overall comparison is shown in Fig. 12 between the constitutive law plots for the parameter sets in Tables 1 and 2, for both materials. The most striking point apparent here is the very high level of general consistency, with all of these curves lying approximately within a 10% band in both cases. In detail, deeper indentation does appear to give slightly better agreement with the tensile data for the AR-Cu, whereas this is not observed for the Ann-Cu. These are, however, minor variations. In general, accepting that ±5% consistency for any stress-strain data is about as accurate as any (uniaxial testing) procedure is likely to yield, it is clear that the methodology presented here is reliable and robust, provided certain conditions are met regarding the accuracy and nature of the original indentation data and the way that they are processed.

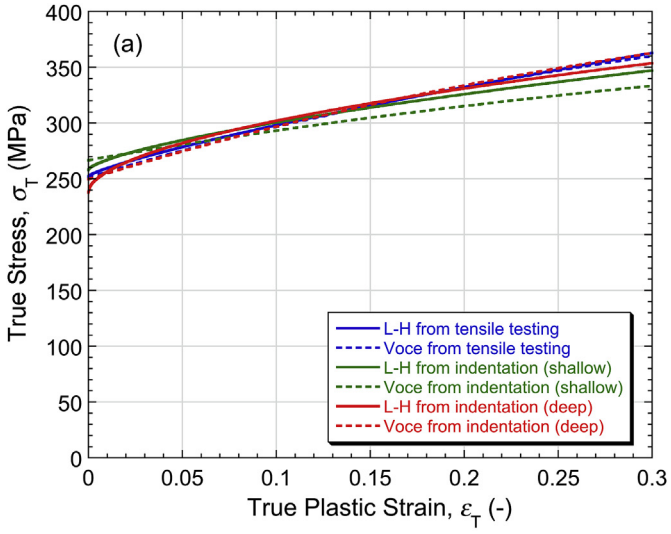

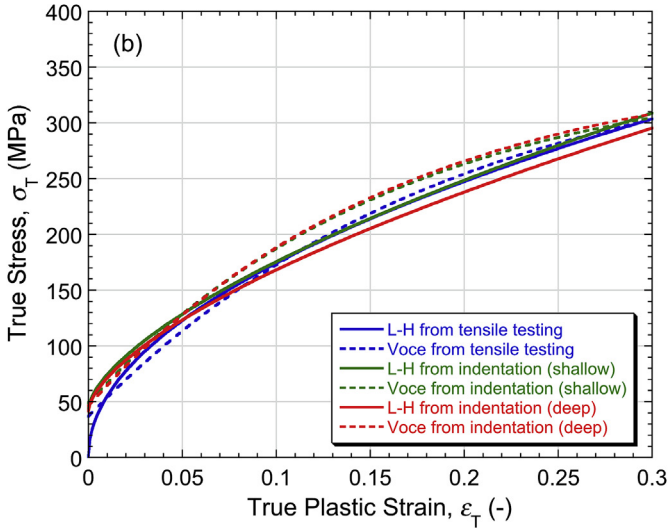

Fig. 12. Comparisons between true stress – true (plastic) strain plots corresponding to the sets of constitutive law parameters in Tables 1 and 2, obtained via Nelder-Mead convergence on tensile or indentation data, for (a) AR-Cu and (b) Ann-Cu.

6. Conclusions

The following conclusions can be drawn from this work:

(a) Iterative FEM simulation of the indentation process has been carried out, primarily using a target outcome of the residual indent profile, with a goodness of fit parameter being used to guide an automated Nelder-Mead convergence algorithm. The coefficient of friction was fixed at 0.2 (with some evidence presented to support this). The study covers two different materials, which exhibit low and high rates of work hardening.

(b) There is a focus on the pros and cons of using residual indent profiles or load-displacement data as the target outcome. It is concluded that, in addition to practical advantages of using profilometry, which include elimination of displacement measurement during a test (and also associated compliance corrections), the profile is more sensitive to plasticity parameter values than the load-displacement plot. This tends to result in slightly more rapid convergence and more accurate inferred stress-strain curves. Moreover, this difference becomes more significant at shallower penetration ratios. The effect of this is that a penetration ratio of, say, 20–25% may be sufficient when using profilometry data, whereas a value of around 40% might be needed to give comparable efficiency with load-displacement data. This in turn reduces the load requirement and, for *in situ* testing, ensures that the indent left in the component is smaller.

(c) A picture is now emerging of how this testing should be done. While a conventional (tensile) testing facility (but not a "nanoindenter") could be used, a customised (bench top) set-up is likely to be best, with dimensions and appearance similar to that of a hardness tester. A basic version could simply have a capability for selecting one of a small number of loads (as with hardness machines), although those should extend up to several kN (whereas many hardness testers allow maximum loads of only ~0.1 kN). The indenter itself is likely to be a (cermet) sphere of diameter 1–2 mm. Another key requirement is a profilometry capability. Of course, the system would be more versatile if it also incorporated a displacement measuring capability.

(d) Comparisons between indentation plastometry outcomes and corresponding data from conventional uniaxial (tensile or compressive) testing are clearly important. A key outcome of plastometry is a nominal stress v. nominal strain plot, obtained by FEM modeling of a tensile test, using inferred plasticity parameter values. Such plots should be reliable with regard to yield stress, subsequent (apparent) work hardening characteristics and the ultimate tensile strength (nominal stress at the onset of necking). It will also be possible to predict the (nominal) strain at the onset of necking, although this is rather sensitive to the precise work hardening characteristics, particularly for materials with relatively low work hardening rates. Prediction of the (apparent) strain at final fracture is problematic, since it is very sensitive to the way that the neck develops and ruptures. The necking down process creates very large local strains (commonly promoting cavitation) and cannot reliably be modeled using indentation-inferred plasticity characteristics. However, this is not a "property" of any real significance.

(e) Accurate comparison between indentation-derived stress-strain curves and those obtained during compressive uniaxial testing requires care. While the strain field within the gauge length during a tensile test should be uniform up to the onset of necking, this is unlikely to be the case during compressive testing, even during the early stages. This is because it is virtually impossible to eliminate friction, which leads to at least some degree of barrelling. Furthermore, displacement measurement data tend to be influenced by "bedding down" effects, particularly in the presence of lubricant. In general, indentation-derived predictions are likely to be more reliable for uniaxial tensile behaviour, which of course also allows the "strength" (UTS) to be assessed.

(f) Indentation plastometry does, of course, require a software package in order to infer stress-strain curves from experimental indentation data. Such packages are now starting to become available - for example, see https://www.plastometrex.com/.

Acknowledgements

This work is supported by EPSRC (grant EP/I038691/1). There has also been extensive input from AWE, as part of an ongoing collaboration with the Gordon Laboratory in Cambridge, aimed at the development of robust and user-friendly tools for the extraction of mechanical property characteristics from indentation data. The authors are particularly grateful to Giles Aldrich-Smith and Nigel Park, for their collaboration and support. There is also ongoing collaboration with a number of other industrial partners, including Richard Green (Solar Turbines), Jon Douglas (Frazer-Nash), Shiladitya Paul (TWI) and David Eaves (Westinghouse).

Appendix A. Supplementary data

Supplementary data to this article can be found online at https://doi.org/10.1016/j.actamat.2019.02.006.

References

[1] C. Heinrich, A.M. Waas, A.S. Wineman, Determination of material properties using nanoindentation and multiple indenter tips, Int. J. Solids Struct. 46 (2009) 364–376.
[2] J. Dean, J.M. Wheeler, T.W. Clyne, Use of quasi-static nanoindentation data to obtain stress-strain characteristics for metallic materials, Acta Mater. 58 (2010) 3613–3623.
[3] D.K. Patel, S.R. Kalidindi, Correlation of spherical nanoindentation stress-strain curves to simple compression stress-strain curves for elastic-plastic isotropic materials using finite element models, Acta Mater. 112 (2016) 295–302.
[4] J. Dean, T.W. Clyne, Extraction of plasticity parameters from a single test using a spherical indenter and FEM modelling, Mech. Mater. 105 (2017) 112–122.
[5] J.E. Campbell, R.P. Thompson, J. Dean, T.W. Clyne, Experimental and computational issues for automated extraction of plasticity parameters from spherical indentation, Mech. Mater. 124 (2018) 118–131.
[6] L. Meng, P. Breitkopf, B. Raghavan, G. Mauvoisin, O. Bartier, X. Hernot, On the study of mystical materials identified by indentation on power law and Voce hardening solids, Int. J. Mater. Form. (2018), https://doi.org/10.1007/s12289-018-1436-1.
[7] P. Hausild, A. Materna, J. Nohava, On the identification of stress-strain relation by instrumented indentation with spherical indenter, Mater. Des. 37 (2012) 373–378.
[8] G. Pintaude, A.R. Hoechele, Experimental analysis of indentation morphologies after spherical indentation, Mater. Res. 17 (2014) 56–60.
[9] J. Isselin, A. Iost, J. Golek, D. Najjar, M. Bigerelle, Assessment of the constitutive law by inverse methodology: small punch test and hardness, J. Nucl. Mater. 352 (1–3) (2006) 97–106.
[10] S. Swaddiwudhipong, J. Hua, E. Harsono, Z.S. Liu, N.S.B. Ooi, Improved algorithm for material characterization by simulated indentation tests, Model. Simulat. Mater. Sci. Eng. 14 (8) (2006) 1347–1362.
[11] I. Peyrot, P.O. Bouchard, R. Ghisleni, J. Michler, Determination of plastic properties of metals by instrumented indentation using a stochastic optimization algorithm, J. Mater. Res. 24 (3) (2009) 936–947.
[12] J. Chen, H.N. Chen, J. Chen, Evaluation of mechanical properties of structural materials by a spherical indentation based on the representative strain-an improved algorithm at great depth ratio, Acta Metall. Sin.-Engl. Lett. 24 (5) (2011) 405–414.
[13] Y. Sun, S. Zheng, T. Bell, J. Smith, Indenter tip radius and load frame compliance calibration using nanoindentation loading curves, Phil. Mag. Lett. 79 (9)

(1999) 649–658.
[14] C. Ullner, E. Reimann, H. Kohlhoff, A. Subaric-Leitis, Effect and measurement of the machine compliance in the macro range of instrumented indentation test, Measurement 43 (2) (2010) 216–222.
[15] K.J. Van Vliet, L. Prchlik, J.F. Smith, Direct measurement of indentation frame compliance, J. Mater. Res. 19 (1) (2011) 325–331.
[16] J.E. Campbell, T. Kalfhaus, R. Vassen, R.P. Thompson, J. Dean, T.W. Clyne, Mechanical properties of sprayed overlayers on superalloy substrates, obtained via indentation testing, Acta Mater. 154 (2018) 237–245.
[17] J. Lee, C. Lee, B. Kim, Reverse analysis of nano-indentation using different representative strains and residual indentation profiles, Mater. Des. 30 (9) (2009) 3395–3404.
[18] W.Z. Yao, C.E. Krill, B. Albinski, H.C. Schneider, J.H. You, Plastic material parameters and plastic anisotropy of tungsten single crystal: a spherical microindentation study, J. Mater. Sci. 49 (10) (2014) 3705–3715.
[19] H.S. Kim, S.H. Kim, W.S. Ryu, Finite element analysis of the onset of necking and the post-necking behaviour during uniaxial tensile testing, Mater. Trans. 46 (10) (2005) 2159–2163.
[20] E.I. Samuel, B.K. Choudhary, K.B.S. Rao, Inter-relation between true stress at the onset of necking and true uniform strain in steels - a manifestation of onset to plastic instability, Mater. Sci. Eng. a-Struct. Mater. Prop. Microstruct. Process. 480 (1–2) (2008) 506–509.
[21] Z.P. Guan, Quantitative analysis on the onset of necking in rate-dependent tension, Mater. Des. 56 (2014) 209–218.
[22] Z.H. Yao, D.Q. Mei, H. Shen, Z.C. Chen, A friction evaluation method based on barrel compression test, Tribol. Lett. 51 (3) (2013) 525–535.
[23] J. Zhou, P. He, J.F. Yu, L.J. Lee, L.G. Shen, A.Y. Yi, Investigation on the friction coefficient between graphene-coated silicon and glass using barrel compression test, J. Vac. Sci. Technol. B 33 (3) (2015).
[24] X. Wang, H. Li, K. Chandrashekhara, S.A. Rummel, S. Lekakh, D.C. Van Aken, R.J. O'Malley, Inverse finite element modeling of the barreling effect on experimental stress-strain curve for high temperature steel compression test, J. Mater. Process. Technol. 243 (2017) 465–473.
[25] M. Fardi, R. Abraham, P.D. Hodgson, S. Khoddam, A new horizon for barreling compression test: exponential profile modeling, Adv. Eng. Mater. 19 (11) (2017).
[26] M. Bol, R. Kruse, A.E. Ehret, On a staggered iFEM approach to account for friction in compression testing of soft materials, J. Mech. Behav. Biomed. Mater. 27 (2013) 204–213.
[27] G. Torrente, Numerical and experimental studies of compression-tested copper: proposal for a new friction correction, Mater. Res.-Ibero-Am. J. Mater. 21 (4) (2018).
[28] X.G. Fan, Y.D. Dong, H. Yang, P.F. Gao, M. Zhan, Friction assessment in uniaxial compression test: a new evaluation method based on local bulge profile, J. Mater. Process. Technol. 243 (2017) 282–290.
[29] D. Duran, C. Karadogan, Determination of coulomb's friction coefficient directly from cylinder compression tests, Strojniski Vestnik-J. Mech. Eng. 62 (4) (2016) 243–251.
[30] A.E. Giannakopoulos, S. Suresh, Determination of elastoplastic properties by instrumented sharp indentation, Scripta Mater. 40 (10) (1999) 1191–1198.
[31] B. Taljat, G.M. Pharr, Development of pile-up during spherical indentation of elastic-plastic solids, Int. J. Solids Struct. 41 (14) (2004) 3891–3904.
[32] V. Karthik, P. Visweswaran, A. Bhushan, D.N. Pawaskar, K.V. Kasiviswanathan, T. Jayakumar, B. Raj, Finite element analysis of spherical indentation to study pile-up/sink-in phenomena in steels and experimental validation, Int. J. Mech. Sci. 54 (1) (2012) 74–83.
[33] J. Dean, G. Aldrich-Smith, T.W. Clyne, Use of nanoindentation to measure residual stresses in surface layers, Acta Mater. 59 (7) (2010) 2749–2761.
[34] J.L. Reed, J. Dean, G. Aldrich-Smith, T.W. Clyne, A methodology for obtaining plasticity characteristics of metallic coatings via instrumented indentation, Int. J. Solids Struct. 80 (2016) 128–136.
[35] M. Burley, J.E. Campbell, J. Dean, T.W. Clyne, Johnson-Cook parameter evaluation from ballistic impact data via iterative FEM modelling, Int. J. Impact Eng. 112 (2018) 180–192.
[36] J.A. Nelder, R. Mead, A simplex method for function minimization, Comput. J. 7 (4) (1965) 308–313.
[37] F.C. Gao, L.X. Han, Implementing the Nelder-Mead simplex algorithm with adaptive parameters, Comput. Optim. Appl. 51 (1) (2012) 259–277.
[38] T.E. Oliphant, Python for scientific computing, Comput. Sci. Eng. 9 (3) (2007) 10–20.
[39] S. van der Walt, S.C. Colbert, G. Varoquaux, The NumPy array: a structure for efficient numerical computation, Comput. Sci. Eng. 13 (2) (2011) 22–30.